

Preparation and photoelectrochemical characterization of WO_3/TiO_2 nanotube array electrode

Jing Wang · Yanhe Han · Manzhi Feng ·
Jinzhu Chen · Xinjun Li · Shanqing Zhang

Received: 25 May 2010/Accepted: 23 August 2010/Published online: 11 September 2010
© Springer Science+Business Media, LLC 2010

Abstract WO_3/TiO_2 nanotube array electrode was fabricated by incorporating WO_3 with TiO_2 nanotube array via a wet impregnation method using ammonium tungstate as the precursor. TiO_2 and WO_3/TiO_2 nanotube arrays were characterized by field emission scanning electron microscopy, X-ray diffraction, and energy dispersive X-ray analysis. In order to characterize the photoelectrochemical properties of WO_3/TiO_2 electrode, electrochemical impedance spectroscopy, and steady-state photocurrent (i_{ss}) measurement at a controlled potential were performed in the supporting electrolyte containing different concentrations of glucose. The photoelectrochemical characterization results reveal that WO_3/TiO_2 nanotube array electrode possesses a much higher separation efficiency of the photogenerated electron–hole pairs and could generate more photoholes on the electrode surface compared with the pure TiO_2 nanotube array electrode. The i_{ss} for glucose oxidation at WO_3/TiO_2 nanotube array electrode is much higher than that at the pure TiO_2 nanotube array electrode.

Introduction

Highly ordered and vertically oriented TiO_2 nanotube arrays fabricated by direct anodization of titanium offer a large surface area with an associated increase in geometric and structural order [1–3]. Owing to the remarkable charge transport property and superior oxidation ability, TiO_2 nanotube arrays have been applied in many fields, such as sensor [4–6], dye sensitized solar cell [7, 8], hydrogen generation by water photoelectrolysis [8, 9], and also the degradation of organic pollutants [10–13]. However, the low photon conversion efficiency is still a major barrier restricting the practical application of TiO_2 nanotube arrays. The modifications on TiO_2 semiconductor such as doping with other elements, coupling with other semiconductors are potentially effective approaches to resolve this problem. The doping of metal or nonmetal elements, such as Fe [14], Sn [15], Zr [16], or N [17] is commonly used to improve the photocatalytic activity of TiO_2 nanotube arrays. The photocatalytic activity of TiO_2 nanotube arrays has also been improved by coupling with the semiconductors such as Fe_2O_3 [18], CdS [19, 20], SnO_2 [21], ZnO , [22] and ZrO_2 [23]. Since WO_3 has a slightly lower conduction band than TiO_2 , the photoelectrons are prone to transfer from the conduction band of TiO_2 to that of WO_3 and result in the effective charge carrier separation when TiO_2 nanotube array is coupled with WO_3 [24–26]. It has been reported that TiO_2 nanotube arrays coupled with WO_3 possess enhanced electrochromic properties and a significantly lower threshold voltage [27]. However, to the best of our knowledge, the photoelectrocatalytic behavior of WO_3/TiO_2 nanotube array has not been reported.

In this study, TiO_2 nanotube array was synthesized via titanium anodization in HF solution, and WO_3 was incorporated onto the resultant TiO_2 nanotube array via wet

J. Wang · M. Feng · J. Chen · X. Li (✉)
Guangzhou Institute of Energy Conversion, Chinese Academy of Sciences, 510640 Guangzhou, People's Republic of China
e-mail: lixj@ms.giec.ac.cn

Y. Han · S. Zhang
Environmental Futures Centre and Griffith School of Environment, Gold Coast Campus, Griffith University, Gold Coast, QLD 4222, Australia

J. Wang
Graduate University of the Chinese Academy of Sciences, 100049 Beijing, People's Republic of China

impregnation method. The effects of WO_3 on the characteristics of TiO_2 nanotube array electrode were investigated by comparing the photoelectrocatalytic oxidation efficiencies of water and organic compounds (i.e., glucose) at WO_3/TiO_2 nanotube array and the pure TiO_2 nanotube array electrodes.

Experimental

Preparation of TiO_2 nanotube array electrode

Titanium sheet (0.2 mm thickness, 99.7% purity) was cut into pieces of $20 \times 50 \text{ mm}^2$. Prior to anodization, the titanium sheet was cleaned with distilled water for 20 min in ultrasonic bath, then it was chemically etched in strong mixed acidic solution of HF and HNO_3 ($\text{HF:HNO}_3:\text{H}_2\text{O} = 1:4:5$ v/v/v) for 2 min to obtain a fresh smooth surface.

The cleaned Ti sheet was anodized in a traditional two-electrode reactor at 20 V for 2 h under stirring conditions at ambient temperature (ca. 23 °C). Anodization experiment was performed in a mixed electrolyte of glycerin and deionized water (1:1 v/v), containing 1 wt% NH_4F . After the anodization, the as-prepared sample was subsequently rinsed with the deionized water and dried in air to obtain a fresh TiO_2 nanotube array sample. The sample was heated at the heating rate of 2 °C/min to 450 °C and annealed for 1 h. Finally, the pure TiO_2 nanotube array electrode was obtained.

Preparation of WO_3/TiO_2 nanotube array electrode

WO_3/TiO_2 nanotube array electrode was prepared by incorporating WO_3 onto TiO_2 nanotube array via wet impregnation process using ammonium tungstate as the precursor. The fresh TiO_2 nanotube array sample was dipped into a 1 mM ammonium tungstate aqueous solution for 2 h. Then, the sample was washed with the deionized water and dried in air. Finally, the sample was heated at the heating rate of 2 °C/min to 450 °C and annealed for 1 h.

Characterization of the nanotube arrays

The crystalline phase of the nanotube arrays was investigated with an X-ray diffractometer using $\text{CuK}\alpha$ irradiation. The morphology of the nanotube arrays was characterized using a field emission scanning electron microscope (FESEM) operated at 5 kV (LEO 1530 VP, Germany). Energy dispersive X-ray (EDX) spectrometer (Inca 300, Oxford, UK) fitted to electron microscope was used for elemental analysis.

Photoelectrochemical cell apparatus and measurements

All the photoelectrochemical experiments were carried out in a three-electrode electrochemical cell with a quartz window for UV illumination. The working electrode surface area exposed to electrolyte was confined by an electrode holder with a 3 mm diameter round opening. The pure TiO_2 or WO_3/TiO_2 nanotube electrode, a saturated Ag/AgCl electrode, and a platinum sheet were used as the working electrode, reference electrode, and counter electrode, respectively. About 0.1 M NaNO_3 aqueous solution was employed as the supporting electrolyte. The volume of the electrolyte was 100 mL. The concentrations of glucose were adjusted in situ by carefully injecting the calculated amount of glucose solution into the reaction media. Illumination was carried out using a 300 W Xenon arc lamp light source filtered by an UV band pass filter (UG-5, Schott). The light intensity was 6.7 mW/cm². Electrochemical characterization, electrochemical impedance spectroscopy (EIS), and steady-state photocurrent (i_{ss}), was measured by CHI660 electrochemical workstation (CH Instruments, USA).

Results and discussions

Structure characterization

Figure 1 shows the X-ray diffraction (XRD) patterns of Ti sheet (curve a), TiO_2 nanotube array (curve b), and WO_3/TiO_2 nanotube array (curve c) annealed at 450 °C for 1 h. For the control purpose, the XRD of pure Ti is also measured (see curve a). The typical patterns of the anatase phase besides the peaks of Ti metal (JCPDs card: 84-1286) can be observed in curve b and curve c, but no any peaks of other TiO_2 phase have been observed, which indicates that only the anatase is obtained under the calcination at 450 °C. The diffraction peaks of WO_3 can be observed after TiO_2 nanotube array incorporated with WO_3 , i.e., the diffraction peaks of WO_3 at 23.15°, 23.61°, and 24.37° can be indexed to (002), (020), and (200) of the monoclinic WO_3 phase, respectively. This suggests that the wet impregnation method could effectively incorporate WO_3 onto TiO_2 nanotube array and the impregnation process do not change the crystalline structure of TiO_2 .

In order to investigate the surface morphology of the film electrodes, the top view of the FESEM images of TiO_2 and WO_3/TiO_2 nanotube arrays is shown in Fig. 2. It can be observed that the nanotubes have an average pore diameter of 100 nm and the wall thickness of ca. 15 nm. The nanotubes are aligned vertically and orderly. The walls of TiO_2 nanotubes are mainly covered by WO_3 nanoparticles. Interestingly, WO_3 can be little observed in the TiO_2

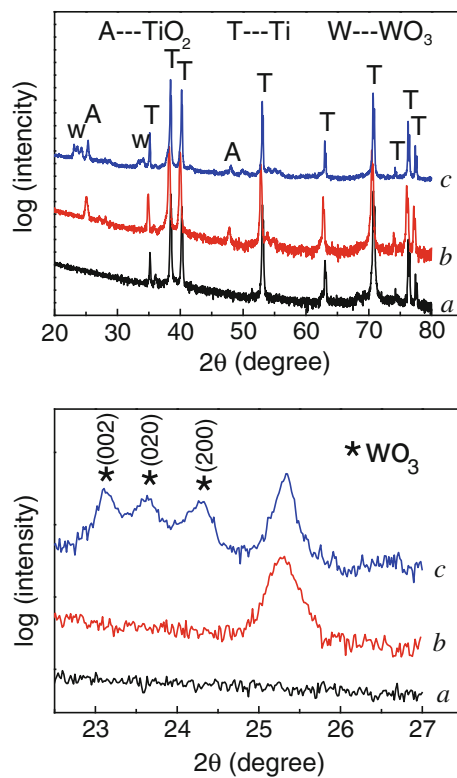


Fig. 1 The X-ray diffraction patterns: **a** Ti sheet; **b** the pure TiO_2 nanotube array, and **c** WO_3/TiO_2 nanotube array annealed at 450°C for 1 h

nanotube pores. It may be because the surface tension of TiO_2 nanotube could block ammonium tungstate solution to flow into the pore. Figure 2 also shows that the morphology of TiO_2 nanotube array is completely maintained, indicating that the TiO_2 nanotube array is so robust that the nanostructure has not been affected by the WO_3 wet impregnation process.

Figure 3 shows the EDX spectrum of the WO_3/TiO_2 nanotube array. The M_α peak of W can be seen clearly at 1.77 keV. Besides the strong K_α and K_β peaks of Ti element appear at 4.51 and 4.92 keV, a moderate K_α peak of the element O can also be observed at 0.52 keV. This further confirms that the nanotube array is made of WO_3 and TiO_2 .

Electrochemical characterization

Electrochemistry offers a powerful tool to explore photoelectrochemical properties, such as the electron transport properties at various electrode surfaces. EIS Nyquist plots are commonly used to investigate the charge transfer resistance and the separation efficiency between the photoelectrons and photoholes [28]. The size of arc radius on the EIS Nyquist plot indicates the rate of the photoelectrochemical reaction on the electrode [29], which is

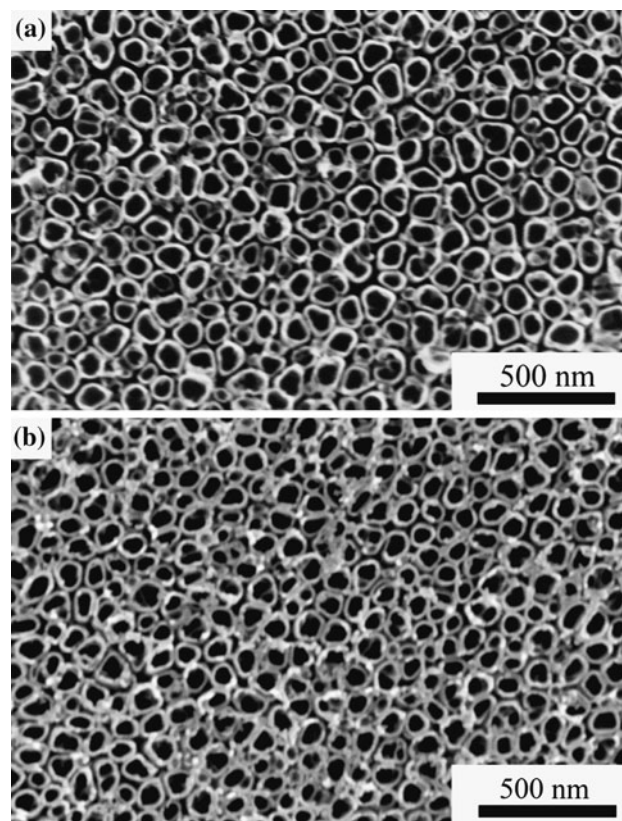


Fig. 2 FESEM images of nanotube arrays: **a** pure TiO_2 nanotube array and **b** WO_3/TiO_2 nanotube array

considered as a useful parameter for characterizing the electron transport resistance in the electrochemical system [30]. Usually, a larger circular radius represents a larger electron transport resistance and a lower separation efficiency of the photoelectrons and photoholes [31]. Figure 4 shows the impedance spectra of the pure TiO_2 and WO_3/TiO_2 nanotube array electrodes under UV illumination in the 0.1 M NaNO_3 aqueous solution. The frequencies for EIS measurement are in the range from 10^5 to 0.01 Hz. As shown in Fig. 4, the circular radius of WO_3/TiO_2 nanotube electrode ($R_{\text{WO}_3/\text{TiO}_2}$) is significantly less than that of TiO_2 nanotube array electrode, indicating that WO_3/TiO_2 nanotube array electrode has lower charge transport resistance and higher separation efficiency of the photoelectrons and photoholes compared with TiO_2 nanotube array electrode.

Photoelectrochemical oxidation of glucose

Under UV illumination, the organic compounds can be readily oxidized by TiO_2 electrode besides water. The general equation for complete mineralization of an organic compound, $\text{C}_y\text{H}_m\text{O}_n\text{N}_k\text{X}_q$, on a TiO_2 electrode can be represented by Eq. 1:

Fig. 3 EDX spectrum of WO_3/TiO_2 nanotube array

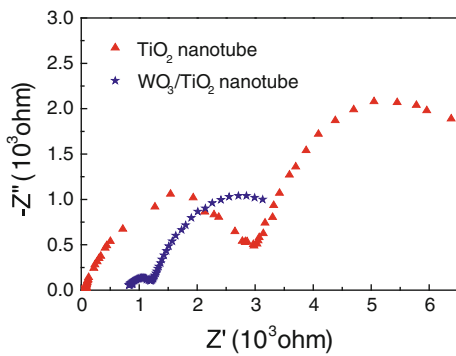
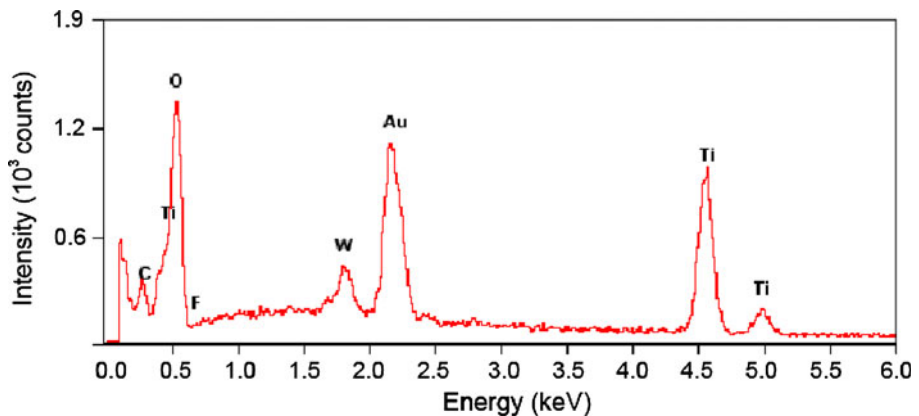
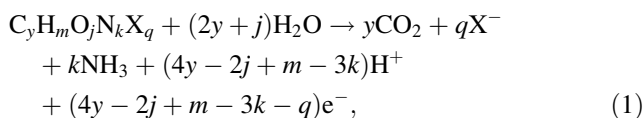


Fig. 4 EIS Nyquist plots of TiO_2 and WO_3/TiO_2 nanotube array electrodes under UV illumination



where N and X represent the nitrogen and halogen atom, respectively. The numbers of carbon, hydrogen, oxygen, nitrogen, and halogen atoms in the organic compound are represented by y , m , j , k , and q , respectively. The electron transfer number (n) in the complete mineralization of the organic compound is equal to $(4y - 2j + m - 3k - q)$. Moreover, according to the semi-empirical treatment of steady-state mass transfer method, under the diffusion control condition, the photocurrent can be given by Eq. 2:

$$i_{ss} = \frac{nFADC}{\delta}, \quad (2)$$

where, n is the number of electrons transferred for the mineralization of organic compounds, which is equal to $(4y - 2j + m - 3k - q)$. F is the Faraday constant, A is the apparent surface area of the electrode, D and δ refer to the diffusion coefficient of an organic compound and the thickness of the effective diffusion layer, respectively, and C is the bulk concentration of the organic compounds. Therefore, the photocurrent obtained in the organic

compounds oxidation directly represents the photoelectrocatalytic activity and effectiveness of oxidation process.

The overall steady-state photocurrent measured in the experiment (i_{ss}) is generally composed of two parts: one part (i_{net}) coming from the oxidation of organic species (i.e., glucose) and the other part (i_{blank}) coming from the oxidation of water. The i_{net} can be calculated by subtracting i_{blank} in electrolyte without organic compounds from i_{ss} in electrolyte with organic compounds according to Eq. 3. For given experimental conditions, i_{net} can be used to represent the oxidation rate of the organic species and therefore the photoelectrocatalytic efficiency of the TiO_2 electrode.

$$i_{net} = i_{ss} - i_{blank}. \quad (3)$$

Effect of potential bias on the i_{blank}

It is well known that applied potential bias can effectively separate the photoelectrons and photoholes generated under light illumination, and also promote the collection efficiency of photoelectrons [31]. Figure 5 shows the relationship between the blank photocurrents (i_{blank}) of TiO_2 and WO_3/TiO_2 nanotube array electrodes and the potential bias with the range from 0 to 1.5 V. As shown in Fig. 5, the photocurrent increases with the increasing potential before it levels off to a saturated photocurrent. The linearly rising part of photocurrent is from 0.0 to 0.6 V, similar to the response of a resistor to the potential. This implies that, in this potential range, the electron transport from the electrode interface to the external circuit is the control step among the photoelectrocatalytic process. The saturated part is from 0.6 to 1.5 V, implying that the photoelectrons generated at the electrode surface during the photoelectrocatalytic process could be mostly withdrawn when the potential applied was over 0.6 V. Therefore, the saturated photocurrents at both electrodes could be observed when the potential is greater than 0.6 V, suggesting that the applied potential during the

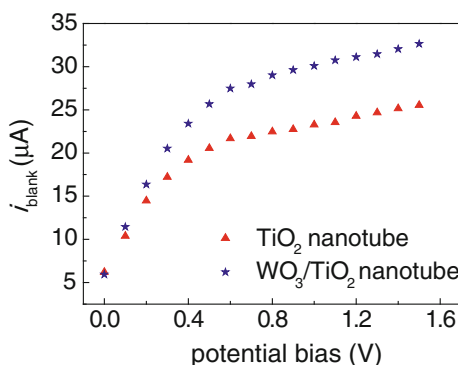


Fig. 5 The effect of the potential bias on i_{blank} of TiO_2 and WO_3/TiO_2 nanotube array electrodes

photoelectrocatalytic oxidation of organic compounds should be more positive than 0.6 V to maximize the photoelectrocatalytic efficiency of these electrodes. Therefore, in order to ensure a sufficient potential bias while minimizing the direct electrochemical reaction, potential bias of 0.8 V was selected for all the subsequent experiments.

Photoelectrochemical oxidation of glucose

In the course of glucose oxidation, the first step involves a bimolecular reaction with the formation of a trapped hole and a surface active radical (e.g., OH^\cdot , O_2^\cdot). The photoelectrochemical oxidation of glucose on TiO_2 and WO_3/TiO_2 nanotube array electrodes was investigated at the constant potential bias of 0.8 V, as shown in Fig. 6. The results show that, for both tested electrodes, the i_{net} increases with the increasing glucose concentration. Moreover, in low glucose concentration range, the changes of i_{net} values are linear with glucose concentrations. While in high glucose concentration range, the i_{net} values deviate from the linear relationship. This is likely due to that the mass transport of organic compounds to the electrode surface is the rate-limiting step at low concentrations but the photoelectrocatalytic reaction at the electrode surface

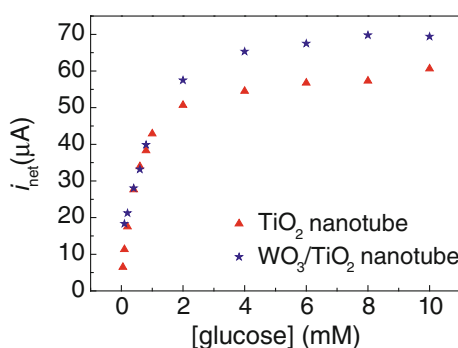


Fig. 6 Relationship between i_{net} and concentration of glucose for TiO_2 and WO_3/TiO_2 nanotube array electrodes

becomes the rate-determining step at high concentrations (see Eq. 2). Most important of all, WO_3/TiO_2 nanotube array electrode possesses higher i_{net} value in the high concentration range (greater than 2 mM glucose), compared with TiO_2 nanotube array electrode. This suggests that the photoelectrocatalytic reaction of glucose on the surface of WO_3/TiO_2 nanotube array electrode is faster than that on the surface of TiO_2 nanotube array electrode. In other words, WO_3/TiO_2 nanotube array electrode has a higher photoelectrocatalytic activity for glucose compared with TiO_2 nanotube array electrode.

Owing to the different band gap and band edge between WO_3 and TiO_2 , when WO_3/TiO_2 nanotube array electrode is excited by UV light, the photogenerated electrons are prone to transfer from the conduction band of TiO_2 to that of WO_3 and result in the effective charge carrier separation, which has been testified by the aforementioned results obtained from EIS measurement. The photogenerated electrons can be transferred to the surface of WO_3 rather than undergoing bulk recombination, while the holes would be effectively scavenged by the water or glucose. Meanwhile, the loading WO_3 on the surface of TiO_2 nanotubes facilitates the electron transport in the electrode. Attributed to the separation of photogenerated electrons and holes, WO_3/TiO_2 nanotube array electrode exhibits the improved photoelectrochemical oxidation performance for glucose.

Conclusions

WO_3/TiO_2 nanotube array electrode was fabricated by incorporating WO_3 with TiO_2 nanotube array via a wet impregnation route using ammonium tungstate as the precursor. Compared with the pure TiO_2 nanotube array electrode, WO_3/TiO_2 nanotube array electrode has better separation efficiency of the photoelectron and photoholes and yields a higher steady-state photocurrent for oxidizing glucose. The improved photoelectrochemical oxidation performance of WO_3/TiO_2 nanotube array electrode could be attributed to the more effective separation of photo-generated electrons and holes.

Acknowledgements The study was supported by Knowledge Innovation Program of the Chinese Academy of Sciences (No. KGCX2-YW-343), Natural Science Foundation of Guangdong Province (No. 07000743), and National 973 Project of China (No. 2009CB220002).

References

- Shankar K, Basham JI, Allam NK, Varghese OK, Mor GK, Feng XJ, Paulose M, Seabold JA, Choi KS, Grimes CA (2009) *J Phys Chem C* 113(16):6327

2. Rani S, Roy SC, Paulose M, Varghese OK, Mor GK, Kim S, Yoriya S, LaTempa TJ, Grimes CA (2010) Phys Chem Chem Phys 12(12):2780
3. Grimes CA, Mor GK (2009) TiO₂ nanotube array: synthesis properties, and applications. Springer, Dordrecht
4. Paulose M, Varghese OK, Mor GK, Grimes CA, Ong KG (2006) Nanotechnology 17:398
5. Varghese OK, Yang X, Kendig J, Paulose M, Zeng K, Palmer C, Ong KG, Grimes CA (2006) Sens Lett 4:120
6. Mor GK, Varghese OK, Paulose M, Grimes CA (2003) Sens Lett 1:42
7. Alivov Y, Fan ZY (2010) J Mater Sci 45:2902. doi:[10.1007/s10853-010-4281-2](https://doi.org/10.1007/s10853-010-4281-2)
8. Shankar K, Mor GK, Prakasam HE, Yoriya S, Paulose M, Varghese OK, Grimes CA (2007) Nanotechnology 18:065707
9. Chen SG, Paulose M, Ruan C, Mor GK, Varghese OK, Grimes CA (2006) J Photochem Photobiol A 177:177
10. Costa LL, Prado AGS (2009) J Photochem Photobiol A Chem 201:45
11. Kang XW, Chen SW (2010) J Mater Sci 45:2696. doi:[10.1007/s10853-010-4254-5](https://doi.org/10.1007/s10853-010-4254-5)
12. Zhang ZH, Yuan Y, Liang LH, Cheng YX, Shi GY, Jin LT (2008) J Hazard Mater 158:517
13. Schmidt-Stein F, Hahn R, Gnochowitz JF, Song YY, Shrestha NK, Hirsch A, Schmuki P (2009) Electrochim Commun 11:2077
14. Sun L, Li J, Wang CL, Li SF, Chen HB, Lin CJ (2009) Sol Energy Mater Sol Cells 93:1875
15. Tu YF, Huang SY, Sang JP, Zou XW (2009) J Alloys Compd 482:382
16. Liu HJ, Liu GG, Zhou QX (2009) J Solid State Chem 182:3238
17. Xu JJ, Ao YH, Chen MD, Fu DG (2010) Appl Surf Sci 256:4397
18. Kuang SY, Yang LX, Luo SL, Cai QY (2009) Appl Surf Sci 255:7385
19. Chen SG, Paulose M, Ruan CM, Mor GK, Varghese OK, Kouzoudis D, Grimes CA (2006) J Photochem Photobiol A Chem 177:177
20. Lin CJ, Yu YH, Liou YH (2009) Appl Catal B Environ 93:119
21. Hou LR, Yuan CZ, Peng Y (2007) J Hazard Mater B139:310
22. Wang N, Li XY, Wang YX, Hou Y, Zou XJ, Chen GH (2008) Mater Lett 62:3691
23. Tsuchiya H, Macak JM, Ghicov A, Taveira L, Schmuki P (2005) Corros Sci 47:3324
24. Li XZ, Li FB, Yang CL, Ge WK (2001) J Photochem Photobiol A Chem 141:209
25. Yang HM, Shi RR, Zhang K, Hu YH, Tang AD, Li XW (2005) J Alloys Compd 398:200
26. Ke DN, Liu HJ, Peng TY, Liu X, Dai K (2008) Mater Lett 62:447
27. Benoit A, Paramasivam I, Nah YC, Roy P, Schmuki P (2009) Electrochim Commun 11:728
28. Spagnol V, Sutter E, Debiemme-Chouvy C, Cachet H, Baroux B (2009) Electrochim Acta 54:1228
29. Leng WH, Zhang Z, Zhang JQ, Cao CN (2005) J Phys Chem B 109:15008
30. Zheng JY, Yu H, Li XJ, Zhang SQ (2008) Appl Surf Sci 254:1630
31. Jiang DL, Zhao HJ, Zhang SQ, John R (2003) J Phys Chem B 107:12774